Available online at www.sciencedirect.com
ScienceDirect
Atmospheric Environment 41 (2007) 776–789
ATMOSPHERIC ENVIRONMENT
www.elsevier.com/locate/atmosenv

Demonstration of a global modeling methodology to determine the relative importance of local and long-distance sources

Roland R. Draxler*

Air Resources Laboratories, National Oceanic and Atmospheric Administration, 1315 East West Highway, Silver Spring, MD 20910, USA

Received 31 March 2006; received in revised form 28 August 2006; accepted 30 August 2006

Abstract

A global three-dimensional (3D) transport–dispersion model was used to simulate Krypton-85 (^{85}Kr) background concentrations at five sampling locations along the US east coast during 1982–1983. The samplers were established to monitor the ^{85}Kr plume downwind of the Savannah river plant (SRP), a nuclear fuel reprocessing facility. The samplers were located 300–1000 km downwind of the SRP. In the original analyses of the measurements, a constant background concentration, representing an upper-limit and different for each sampling station, was subtracted from the measurements to obtain the part of the measurement representing the SRP plume. The use of a 3D global model, which includes all major ^{85}Kr sources worldwide, was able to reproduce the day-to-day concentration background variations at the sampling locations with correlation coefficients of 0.36–0.46. These 3D model background predictions, without including the nearby SRP source, were then subtracted from the measured concentrations at each sampler, the result representing the portion of the measurement that can be attributed to emissions from the SRP. The revised plume estimates were a factor of 1.3–2.4 times higher than from the old method using a constant background subtraction. The greatest differences in the SRP plume estimates occurred at the most distant sampling stations.
Published by Elsevier Ltd.

Keywords: Global dispersion model; Long-range transport; Krypton-85; Savannah river plant; ACURATE; HYSPLIT

1. Introduction

Atmospheric dispersion models are commonly designed, evaluated, and tested using measured pollutant air concentration data. For short-range dispersion applications, pollutant air concentrations can be very large and those concentrations can easily be attributed to a specific source, thereby simplifying a model's evaluation. However, at longer transport distances, the concentrations from various pollutant sources mix together and it can become much more difficult to ascertain source attribution information for a specific measured value. Therefore, many researchers have focused on using unique inert atmospheric tracers in their model evaluations (Mosca et al., 1998; Draxler et al., 1991) rather than more commonly measured air pollutants. Extensive long-term measurements are available for many pollutants. The main disadvantages are that these pollutants have numerous emission sources, high or variable background values, and may be subject to various conversion or removal processes. A pollutant used by many

*Tel.: +1 301 713 0295x117; fax: +1 301 713 0119.
E-mail address: roland.draxler@noaa.gov.

1352-2310/$ - see front matter Published by Elsevier Ltd.
doi:10.1016/j.atmosenv.2006.08.052

researchers has been ^{85}Kr because there are few source locations and with some exceptions its emissions are documented (with some uncertainties), long-term sampling data are available, and ^{85}Kr is relatively inert with a long half-life (WMO, 1995). Many of the first generation global chemical models (Weiss et al., 1983; Jacob et al., 1987; Zimmermann et al., 1989; Levin and Hesshaimer, 1996) used ^{85}Kr to evaluate their model's advection and dispersion components.

Extensive measurements of ^{85}Kr were made in the US during the 1970s and 1980s focusing on plumes downwind of the nuclear fuel reprocessing facility at the Savannah river plant (SRP), South Carolina (Pendergast et al., 1979; Telegadas et al., 1980) and the Idaho National Engineering Laboratory, Idaho (Ferber et al., 1977). Although the initial measurements at the SRP were conducted within 150 km of the plant, a subsequent experiment, the Atlantic Coast Unique Regional Atmospheric Tracer Experiment (ACURATE—Heffter et al., 1984) was conducted from March 1982 through September 1983 to test models that simulated long-range transport and dispersion. Five sampling sites were established along the northeast coast of the US from 300 to 1000 km from the plant (Fayetteville, NC to Murray Hill, NJ—see Fig. 1) for the 18 months long experiment. Heffter et al. (1984) subtracted a constant concentration, representing an upper-limit to the background at each sampling location, to determine the part of the measurement that came from the SRP. However, because virtually all of the ^{85}Kr sources are in the northern hemisphere (most of the major sources are in Europe and Asia), there were many smaller fluctuations in the measurements that could be attributed to these sources. This was less of an issue for the samplers near the SRP, but the most distant sampler at Murray Hill was frequently affected by a fluctuating background concentration and low contributions from the SRP.

A numerical solution to the problem of background subtraction was tested by solving the advection–diffusion equation on global three-dimensional (3D) grid. The model was initialized with a measurement-based latitudinal ^{85}Kr gradient in January of 1982 and then run for two years with a continuous emission rate from the known major sources of ^{85}Kr. Although the SRP source was included in the calculation, it was artificially displaced to retain its contribution to the background but remove its influence on the nearby samplers. The 3D model prediction of the ^{85}Kr background concentration at each of the sampling locations and times was then subtracted from the measured concentration. The resulting estimated concentration time series of the SRP plume was then compared with a dispersion model calculation using the published SRP hourly emission rate.

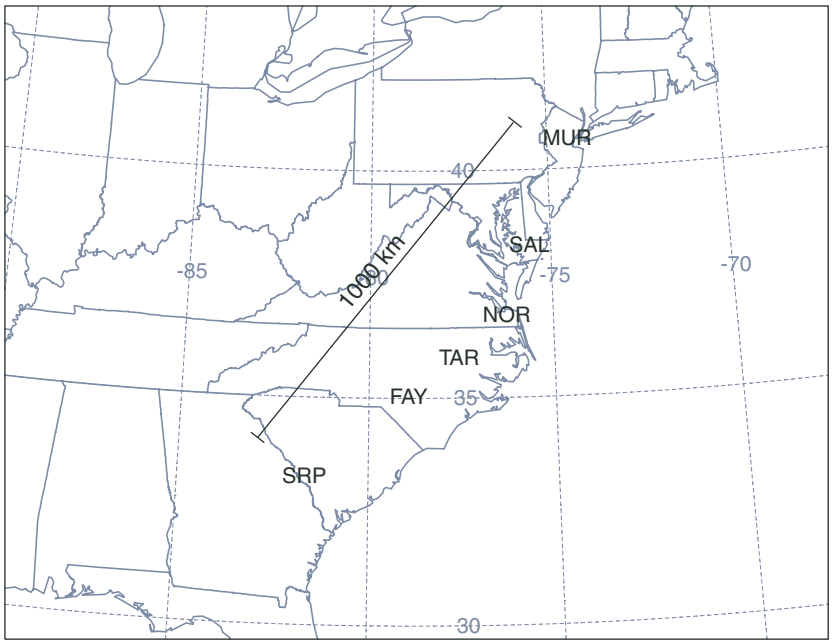

Fig. 1. The location of the source (SRP) and the five sampling locations.

2. Global dispersion model

The design of the global model developed for this application is a considerably simplified version compared to most other models of this genre (Prather et al., 1987; Bey et al., 2001; Horowitz et al., 2004; Winger et al., 2005) consistent with its application to this specific problem. Only one inert species is considered. The meteorological data, obtained from public archives, are used directly in the calculation without spatial or temporal interpolation. However, the meteorological data, given on pressure levels, are interpolated to a sigma-pressure terrain-following coordinate system. Further, it is not necessary to integrate the model from the start of ^{85}Kr emissions in the mid-1940s but just prior to the start of the experiment. Therefore, some of the key issues for global climate models, such as inter-hemispheric exchanges and tropospheric–stratospheric mixing, are minimized in this application because of the short integration duration. As will be shown in the following sections, this considerably simplified computational scheme provides quite good simulation results.

2.1. Model grid configuration

The horizontal concentration grid is configured to match the meteorological data grid at a 2.5° resolution. The grid system indices increase from south to north and from west to east. The system's longitude coordinate system ranges from 0 to 360 or from −180 to 180. The latitude coordinate system ranges from −90° to 90°. Above 70° latitude, the longitude resolution of the concentration grid is coarsened progressively with each grid point closer to the pole because of the decreasing circumpolar distance with latitude. The pole's grid point sits at the center of a circular grid cell. The advection and diffusion algorithms insure that regardless of a cell's shape and neighborhood, the horizontal mass transfer into it is the sum of the fluxes from all the adjacent cells weighted by the area of each neighbor's interface. At the pole the fluxes are averaged along the circumference of the cell.

The vertical coordinate system is on pressure-sigma surfaces. The sigma coordinate system is first defined for the standard pressure levels of the meteorological data assuming a model top (P_t) and surface pressure (P_s) of 10 and 1013 hPa, respectively, using the standard definition for a pressure-sigma coordinate:

$$\sigma = \frac{P - P_t}{P_s - P_t}, \tag{1}$$

where P is the pressure at the data level. The vertical grid, and corresponding meteorological data, consists of 17 levels that define the grid cell center point.

2.2. Equations

The global model for the temporal variation of the ^{85}Kr background concentrations is the solution of the mass conservative advection–diffusion equation

$$\frac{\partial q}{\partial t} = -\left(u\frac{\partial q}{\partial x} + v\frac{\partial q}{\partial y} + w\frac{\partial q}{\partial z}\right) + \left(\frac{\partial}{\partial x}K_H\frac{\partial q}{\partial x}\right) + \left(\frac{\partial}{\partial y}K_H\frac{\partial q}{\partial y}\right) + \left(\frac{\partial}{\partial z}K_V\frac{\partial q}{\partial z}\right) + e - d, \tag{2}$$

where q is the pollutant mass mixing ratio; u, v, and w are the component wind velocities; K is the diffusivity in the horizontal (H) and vertical directions (V); e is the emission rate; and d is the radioactive decay rate (10.76 years). The numerical integration is computed on a regular global latitude–longitude grid (144×73 cells) assuming that the west–east and south–north grid-cell interfaces are orthogonal to each other over the whole domain. The distances between the cells' center points and the areas of the cells' interfaces are computed based upon a spherical earth. The finite difference equations are solved using an upstream difference approximation for the advection terms and a centered difference approximation for the diffusion terms. The vertical gradient of mass is zero across the upper and lower boundaries. Vertical density variations are incorporated implicitly by computing the vertical gradients from the geopotential height differences of the pressure-sigma vertical coordinate and through the conversion of air concentration to mass mixing ratio.

Following Phillips (1986), the vertical diffusion coefficient ($m^2\,s^{-1}$) is computed from

$$K_V = \frac{50}{2 + R_i}, \tag{3}$$

and where the stability is defined by the local Richardson number

$$R_i = \frac{g}{\theta}\frac{\partial\theta/\partial z}{(\partial u/\partial z)^2 + (\partial v/\partial z)^2}, \tag{4}$$

computed from the gradients of potential temperature (θ) and wind speed. In the horizontal, the east–west and north–south diffusion coefficients are assumed to be equal and maintain a constant proportionality according to the grid spacing from the pole to the equator such that

$$K_H(m^2\ s^{-1}) = 2 \times 10^5 D_x/D_y, \quad (5)$$

and where D_x is the east–west grid spacing and D_y is the north–south grid spacing at the computational grid point. The ratio D_x/D_y is just the cosine of the latitude resulting in a decrease of the horizontal mixing coefficient with increased latitude. In the tropical latitudes ($<30^\circ$) the magnitude of the horizontal mixing was doubled to account for the effects of deep convection which would increase the ^{85}Kr flux into the southern hemisphere because of its large inter-hemispheric gradient. The mixing coefficient is comparable to the value (around $10^6\,m^2\,s^{-1}$ near the equator) obtained from enhanced tropical mixing algorithm used by Prather et al. (1987).

2.3. Computational approach

The global dispersion model integration of Eq. (2) uses the meteorological data fields from the National Center's for Environmental Prediction/National Center for Atmospheric Research (NCEP/NCAR) meteorological reanalysis project (Kalnay et al., 1996). These data are available at 2.5° resolution at 6-h intervals (synoptic times) on standard pressure levels from 1948. Reanalysis data are created in a series of steps in which observations are combined with a short-range forecast from the previous analysis in a way to minimize the deviations between the observations and the short-range forecast. The NCEP/NCAR reanalysis was created by a 28 level spectral model, which corresponds to a horizontal grid spacing of about 200 km.

The computational sequence is that the meteorological data fields of surface pressure and the 3D fields (heights of the pressure surfaces, the horizontal and vertical wind components, temperature, and relative humidity) are read into the data arrays at the beginning of each 6 h integration interval centered about the data observation time. All meteorological variables are linearly interpolated from the input constant pressure surfaces to the model's sigma surface (Eq. (1)) on the 2.5° grid. Eq. (2) is integrated with the same meteorological data fields until the next synoptic data time.

The vertical mixing coefficient is computed for each grid interface as well as the maximum integration time step to maintain computational stability. Integration time steps were typically 30 min. Mass continuity is insured by computing the total mass before and after each integration period. The ratio between the two mass totals is applied as a constant multiplication factor over all grid points. Typically, the mass adjustment is on the order of 0.01% per time step. At pre-specified intervals, the mass mixing ratio is converted to concentration at standard temperature and pressure (STP) and the 2D (lowest grid cell) concentration field is saved for subsequent analyses.

2.4. Mass initialization

Fortunately, the ACURATE experiment occurred around the same time as some Atlantic cruise measurements (from Weiss et al., 1983) used by both Jacob et al. (1987) and Winger et al. (2005). The ^{85}Kr latitudinal gradient (from 16.5 pCi m^{-3} at 68°S to 20.3 pCi m^{-3} at 52°N) was measured in January 1982 and those values were used in a regression equation (one for each hemisphere) to compute the ^{85}Kr mass-mixing ratio in each ground-level grid cell based only upon its latitude. The largest gradients occur across the equator. The mean northern and southern hemispheric values were 19.2 and 16.7 pCi m^{-3}, respectively. Following Jacob et al. (1987), the troposphere was initially assumed to be well mixed and the concentrations in the lower and upper stratosphere were set to 0.87 and 0.54, respectively, of the values in the troposphere. All model simulations were started on 1 January 1982 and ran through 31 December 1983. Because ACURATE did not start until March, the model calculation had time to adjust its concentration gradients to reflect the spatial distribution of the actual emissions, thereby providing a more realistic concentration prediction at the start of the experiment.

2.5. Emissions

The 3D model was integrated for a two year simulation using two different emission inventories: the one used by Jacob et al. (1987) which identified eight sources emitting about 240 PBq per year and the more recent compilation by Winger et al. (2005) which identified 14 sources emitting about 300 PBq per year. Hereafter, these inventories will be

abbreviated to J87 and W05. As shown in Table 1, the major difference between the two inventory totals can almost entirely be attributed to the emissions from the former Soviet Union. At the time of the J87 publication, amounts and exact locations for those sources were unknown and were estimated by fitting the model results to the available measured data.

In this application the purpose of the calculation is to estimate the contribution to the measured concentration during ACURATE from sources other than the SRP. Therefore, in all the calculations discussed here, the SRP source will be moved by 180° longitude away from the ACURATE sampling network. In this way the SRP emissions will be added to the global inventory, properly increasing the background values with time, but not affecting the concentrations just downwind of the SRP. This is discussed further in Section 4.

Table 1
The annual emissions (PBq) of ^{85}Kr from the major sources in 1982 and 1983 as used by Jacob et al. (1987) and from a more recent compilation by Winger et al. (2005)

Facility		Lat. (N)	Long.	1982		1983	
				J87	W05	J87	W05
SRP	US	33	81 W	20.7	19.1	25.5	25.8
Idaho	US	43	112 W	0.4	0.3	0.0	0.1
La Hague	FR	49	1 W	47.0	45.1	72.2	50.2
Marcoule	FR	44	5 E	11.5	11.5	11.5	22.9
Chelyabinsk	RU	56	61 E	111.0	89.4	88.8	76.4
Tomsk	RU	57	85 E		48.6		41.5
Krasnoyarsk	RU	56	94 E		39.7		33.9
Sellafield	UK	55	4 W	44.0	44.0	41.8	41.8
Karlsruhe	DE	49	8 E	0.0	0.6	3.0	2.8
Dimona	IS	31	35 E		0.4		0.4
Tokai-Mura	JP	37	141 E	7.0	9.8	3.3	0.5
Tarapur	IN	20	73 E		0.2		0.2
Guangyan	CN	32	106 E		1.0		1.0
Subei	CN	39	97 E		3.0		3.0
Total (PBq)				242	312	246	300

3. Krypton-85 measurements

The ACURATE experiment consisted of measuring ^{85}Kr air concentrations downwind of the SRP, SC. Hourly ^{85}Kr emissions from the SRP are tabulated in the report (Heffter et al., 1984) and are used only for the SRP plume model evaluations (Section 5.2). The emission rate calculated from the hourly source was 17.8 PBq per year (spanning both 1982 and 1983), slightly lower than the values shown in Table 1. The annual average rates reported in Table 1 are used for the 3D model concentration background computation.

Air samples were collected for 19 months (March 1982–September 1983) at five locations along the US east coast from 300 to 1000 km from the plant (see Fig. 1 and Table 2). The original air concentration data were reported in pCi m^{-3} and therefore these units will be used in this analysis. All stations collected 12-h average samples, except at MUH, which collected 24-h samples. The number of collected samples available for evaluation varied from 498 at MUH to 779 at SAL.

The background concentrations (non-SRP contributions) were computed by Heffter et al. (1984) by analyzing the cumulative frequency distribution of the measured concentrations at each station. These results are shown in Fig. 2 for each of the stations and there is a distinct delineation in the slope between background concentrations and plume concentrations. The concentration at the point when the curve started to rapidly slope upward from a quasi-straight line was considered by Heffter et al. (1984) to be the upper limit to the background concentration. This transition generally occurred at around the 90% level. Concentrations

Table 2
The ACURATE sampling stations, the constant upper-limit background concentration as determined by Heffter et al. (1984), and the resulting mean plume concentration and its variance

Station		Latitude (°N)	Longitude (°W)	Background (pCi m^{-3})	Plume (pCi m^{-3})	Variance
Fayetteville, NC	FAY	35.07	78.89	19.0	0.81	14.94
Tarboro, NC	TAR	35.91	77.55	19.0	0.75	24.51
Norfolk, VA	NOR	36.85	76.27	19.1	0.36	6.58
Salisbury, MD	SAL	38.37	75.59	19.2	0.17	1.31
Murray Hill, NJ	MUH	40.68	74.40	19.3	0.17	3.13

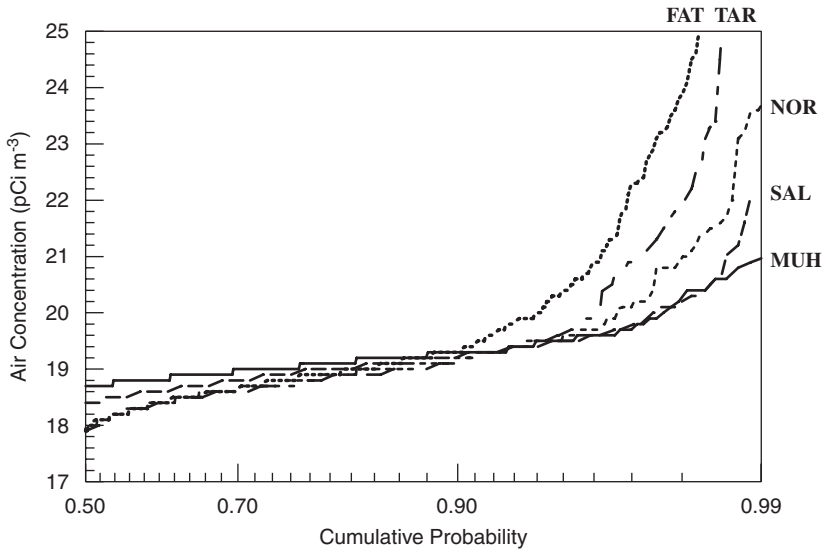

Fig. 2. Cumulative probability distribution of the measured ^{85}Kr air concentration at the five sampling locations.

above this value were considered to be composed entirely of contributions from the SRP, while lower concentrations could be entirely background or a mix of background and small contributions from the SRP.

Except for SAL and MUH, which are comparable, the mean plume concentration (after subtracting a constant upper-limit background) goes down with distance from the source (Table 2). However, the plume variance is more complicated. The variance at TAR is much larger than FAY, presumably because of a greater number of SRP plume events at that sampler. Then variance decreases with distance but goes up again at MUH. Some of the increased variance at MUH is due to the fact that most of the krypton sources are in the northern latitudes and samplers farther north will be more affected by variations in concentration contributions from these other sources, complicating the determination of how much of the measured krypton at MUH is from the SRP and how much is from the other sources.

4. Global model simulation results

The desired end-product is to improve the estimation of the background concentration by using a variable background concentration that accounts for the other more distant sources of krypton not coming from the source of interest. In terms of the ACURATE experiment, the intent is to remove concentration fluctuations that are not due to emissions from the SRP. As mentioned earlier, due to the proximity of the SRP to all of the ACURATE sampling locations (about three model grid cells), SRP emissions would overwhelm the grid cells corresponding to the ACURATE sampling locations. Rather than deleting the SRP emissions from the inventories, the 3D model simulations were run after moving the SRP source location by 180° longitude. In this way the model predictions for the US east coast sampling locations would not be directly influenced by the SRP emissions but the SRP emissions would still contribute to the increasing global krypton-85 inventory.

4.1. Sensitivity to emission inventories

Global 3D model calculations were made using both the J87 and W05 emission inventories and these results are shown in Fig. 3 for the MUH sampling location. MUH was selected for illustration purposes because it has the fewest missing data, it is the furthest from the SRP, and it has a more complicated background signal as evidenced by its larger variance as compared with SAL. The top panel shows the results for 1982 and the bottom panel shows the results for 1983. Calculations using the J87 inventory clearly overlap the measurements while the calculation using the W05 inventory overpredicts the measurements by a slowly varying amount which reaches a maximum near the center

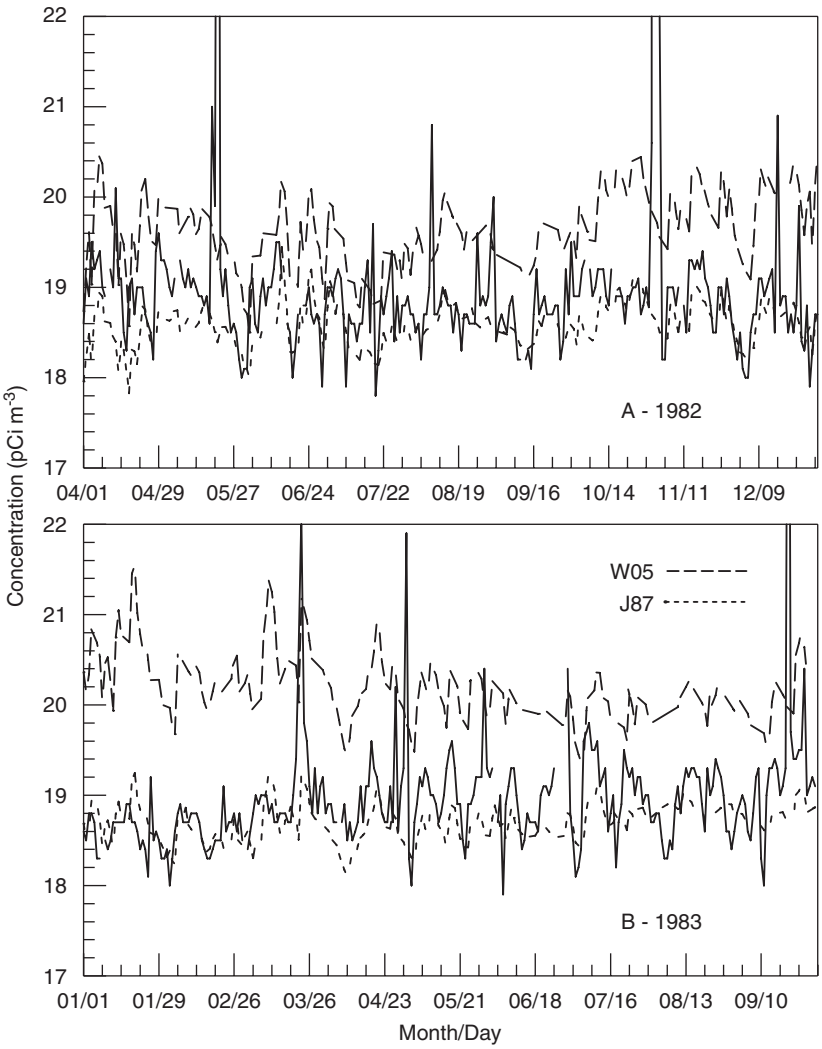

Fig. 3. Concentration time series from April 1982 through September 1983 measured at MUH (solid line), calculated using the J87 emission inventory (dotted line) and the W05 emission inventory (dashed line). Abscissa marks are given at one week intervals. The top panel (A) shows the data for 1982 and the bottom panel (B) shows the data for 1983.

of the period (early 1983). As shown earlier, the main difference between the two inventories are the emissions from Russia, and this result suggests that the earlier Jacob estimate (at least for 1982 and 1983) is closer to correct. Both W05 and J87 compared their model results with measurements during this period and the W05 calculation showed substantial over-prediction in the northern hemisphere which was not evident in the J87 results.

A simple statistical summary of the calculations with the two inventories is shown in Table 3. The 3D calculations are intended to simulate the background concentration. Thus only those measured values below the initially estimated maximum background concentration (19.3 pCi m^{-3}) were compared to the 3D model results. As is evident in Fig. 3, most measured concentrations fall below 19.3 pCi m^{-3}, except for a few isolated peaks,

Table 3
A summary of the 3D model calculation results at MUH using the J87 and W05 emission inventories

	Measured	J87	W05	J87m	J87–W05
Mean (pCi m^{-3})	18.79	18.61	19.86	18.71	18.69
Correlation		0.34	0.26	0.35	0.39

The J87m column uses the monthly emission factors for La Hague and the J87–W05 column uses the J87 inventory only through March 1983. Correlations are computed for the measurements that are below 19.3 pCi m^{-3}.

presumed to be coming from the nearby SRP. From the standpoint of computing an improved background concentration, model bias is not a significant issue because the predictions can easily be adjusted to account for the unknowns of the total global emission inventory. However, properly predicting the day-to-day variations, as indicated by the correlation coefficient is a factor that can significantly affect the resulting calculation of the plume concentrations attributed to any one source.

Additional emission inventory variation tests were conducted to test temporal sensitivity. One major assumption of the background modeling approach used here is that the emissions are assumed to be uniform and continuous. More detailed temporal emissions are not available for most locations. However, W05 obtained monthly emissions for the La Hague facility in France. The monthly values showed reduced emissions during the summer months and correspondingly higher emissions during the winter months. The W05 monthly emission factors were applied to the J87 emission values for La Hague and the 3D model calculation results for MUH using these emissions (the J87m column in Table 3) suggest that there is no substantial difference in performance compared to the calculation using the annual average emission rate. A reduced sensitivity to the monthly emissions is expected due to the large transport distances involved from Europe to the sampling network in the US.

These issues can be explored further by redrawing Fig. 3 with the bias (about 1 pCi m^{-3}) removed from the W05 calculation. The results shown in Fig. 4 divide into three segments. The overall correspondence of day-to-day variations between the W05 and J87 inventory calculations seems good except during the period January–March of 1983. This period shows a systematically higher bias in the W05 calculation not evident before or after that time. During the remainder of 1983, the W05 emissions seem to produce a better fit than the J87 emissions.

In the winter months, the average flow regime over the northeast US is from the north and therefore air masses would be expected to bring higher ''background'' concentrations from European and Asian sources. The fact that the concentrations did not go up early in 1983 as indicated by the model calculation, suggests that the Russian sources were not emitting as much as defined by the W05 inventory but at a rate closer to the J87 inventory.

A complicating factor is that the better correspondence (magnitude of the day-to-day concentration variations) using the W05 inventory during the remainder of 1983 suggests the W05 emission rate was more realistic during that period. This result can also be expressed as the variance, a measure of the strength of the sources contributing to the background. The variance of the measurements and calculations, divided into the three computational periods, is shown in Table 4. During the first two periods the variance of the measurements and calculations using the J87 inventory are comparable while the calculation using the W05 inventory is three to four times as large. During the last period, the best match to the measured variance occurs when using the W05 inventory.

This last result suggests another temporal emission variation calculation is to blend the J87 and W05 inventories by using J87 through March of 1983 and then the W05 inventory for the remainder of the calculation period. This blended result (J87–W05 column in Table 3) actually produced the best correlation at MUH and will be used for the background subtraction.

4.2. Sensitivity to unknown emissions

Sensitivity to the magnitude of the Russian emission sources during January–March of 1983

Table 4
Summary of the 3D model calculation results at MUH in terms of mean concentration and its variance for both emission inventories and for three different time periods compared to the measurements that are below 19.3 pCi m^{-3}

Period	MUH		J87		W05	
	(pCi m^{-3})	Variance	(pCi m^{-3})	Variance	(pCi m^{-3})	Variance
<16/12/82	18.78	0.10	18.44	0.12	19.32	0.46
16/12–26/3	18.63	0.06	18.67	0.05	20.38	0.17
>26/03/83	18.90	0.10	18.71	0.03	20.05	0.08

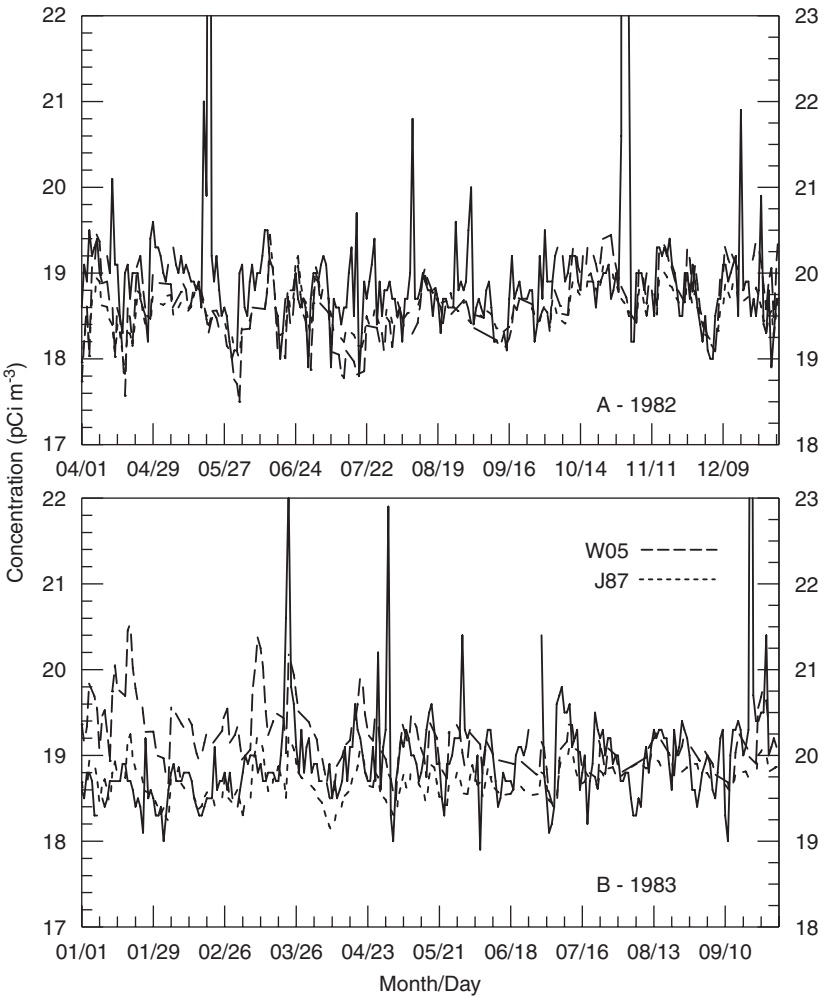

Fig. 4. The same as Fig. 3, except that the calculation using the W05 inventory has been plotted relative to the ordinate scale on the right side offset by 1 pCi m^{-3}.

suggests a series of simulations, each with one of the Russian sources turned off for the entire simulation period. These results are shown in Fig. 5 using the W05 inventory. Eliminating any one Russian source does not lower the calculated concentrations sufficiently to match the measurements. Further, the day-to-day variations of the one-source reduction calculation are comparable to the calculation that includes all the sources, where the magnitude of the variation is much larger than observed in the measurements. Curiously, the calculation with Chelyabinsk turned off resulted in the largest correlation coefficient of any calculation (0.47), and it was the only calculation with a higher correlation than any of those shown in Table 3. Although the total W05 global emissions without Chelyabinsk were slightly less than the J87 emissions, the calculation still showed higher concentrations than the J87 calculation during this period. During the other times (not shown) the two calculations were not substantially different from each other. A calculation with all three Russian sources turned off results in a substantial concentration under-prediction and a concentration time-series with not enough daily variation.

These results suggest that the correct solution is a more complex temporal emission scenario than is represented by either the J87 or W05 inventories and is not likely to be resolved without additional data. One of the main issues related to this problem is that the 3D model calculation assumes a continuous and constant (adjusted each year) emission rate, while the industrial process that results in krypton emissions are far from continuous

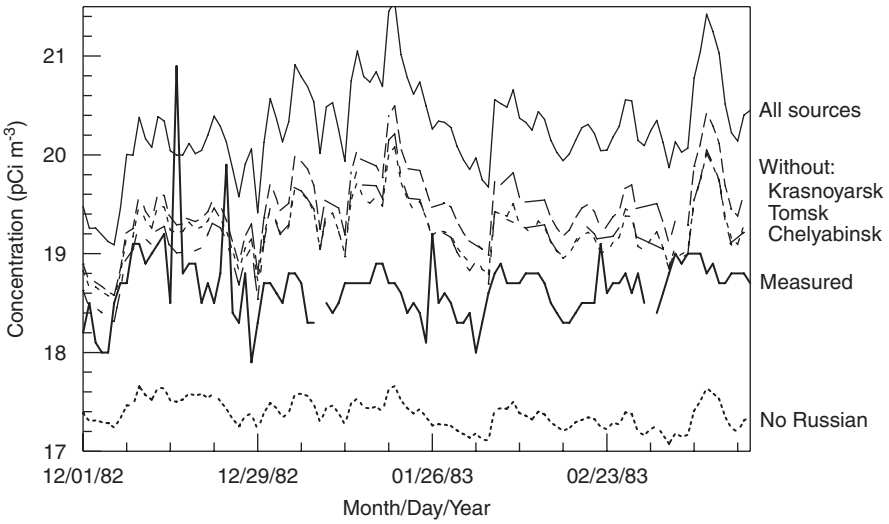

Fig. 5. Concentration time series from December 1982 through February 1983 measured at MUH (bottom solid line), calculated using the W05 emission inventory using all the Russian sources (top solid line), and with various individual sources removed (dashed lines). The lowest dotted line shows the result with all the Russian sources removed.

(e.g. see the hourly rates tabulated by Heffter et al., 1984 during ACURATE). It is unlikely that many of these emission rates will ever be known in any more detail and therefore there will always be some residual uncertainty to a model-based approach, a result also shown by Zimmermann et al. (1989). Further, because this evaluation is only looking at a particular sampling network and short time period, more definitive conclusions about which inventory would be better for longer duration model simulations are not possible.

5. Variable background subtraction

5.1. Global model results

Although it may be possible to construct an emission scenario that further optimizes the results during the ACURATE experiment, the primary purpose of this analysis is to improve upon the constant background subtraction method so that source–receptor modeling approaches can be more effectively applied to the SRP-ACURATE data. In that context, the 3D calculation with the blended J87–W05 inventory is used to estimate the daily background concentrations for each of the ACURATE sampling stations. The overall 3D model statistical results are shown by station in Table 5. Model results are only compared to the measured values that fall below the initial upper-limit background estimate shown in Table 2 because the 3D model calculations do not show the effect of the nearby SRP emissions. The results indicate that the 3D model performs slightly better at the more southern stations, most likely because they are further away from the major krypton sources all clustered in the higher latitudes.

Table 5
A summary of the 3D model calculation results using the J87–W05 inventory blend compared to the below-background measurements as defined in Table 2

Station	Measured ($pCi\,m^{-3}$)	Calculated ($pCi\,m^{-3}$)	Correlation
FAY	18.45	18.47	0.44
TAR	18.46	18.43	0.46
NOR	18.55	18.56	0.44
SAL	18.64	18.59	0.36
MUH	18.79	18.68	0.39

All values were averaged over the experimental period at each ACURATE station.

Using the 3D model calculation results, a new "measured plume" time series was constructed for each station by subtracting the corresponding model calculation from the measurement. The mean plume concentrations are shown in Table 6 for the original constant upper-limit background, a constant background representing a median background ($0.5\,pCi\,m^{-3}$ less than the upper-limit background), and the new variable background subtraction result. As expected from the concentration distribution shown in Fig. 2, where 90% of the

Table 6
Average plume concentrations attributed to emissions from the SRP during ACURATE using the original constant background subtraction (Table 2), the median background subtraction (Table 2 value minus 0.5 pCi m^{-3}), and the new variable background subtraction (from the 3D model)

Station	Constant (pCi m^{-3})	Median (pCi m^{-3})	Variable (pCi m^{-3})	Ratio
FAY	0.81	1.05	1.04	1.28
TAR	0.75	0.97	0.98	1.31
NOR	0.36	0.56	0.57	1.58
SAL	0.17	0.35	0.39	2.29
MUH	0.17	0.33	0.40	2.35

The concentration ratio of the variable method to the original constant method is shown in the last column.

measurements are less than the constant upper-limit background value, the new plume estimates using the variable background method show much higher average concentrations, differences increasing with distance from the SRP. At MUH, the new average SRP plume estimate is higher by over a factor of two. The median constant background approach, because of its lower concentrations, produces a result more comparable to the variable background method. The difference between the constant and variable background mean plume concentrations ranges from 0.21 to 0.23 pCi m^{-3} for all the samplers. As noted earlier, bias can be attributed inaccuracies in the emission inventory. However, the fact that the bias is constant with latitude suggests that the model itself has not introduced any bias that cannot be compensated into this approach. Although the average plume concentrations using the median constant background and the variable background appear comparable, they may not identify the same low-concentration plumes from the SRP. This will be addressed in the next section.

5.2. Lagrangian dispersion model performance

ACURATE was conducted to evaluate long-range dispersion models. A simple test of the new measured plume estimates would be to compare them to the results from a dispersion model calculation using the hourly SRP emission rates. Presumably once the variations introduced by the other un-modeled sources has been removed from the measurements the remaining concentration variations are only due to variations introduced by advection, dispersion, and temporal variations in the emission rate from the SRP. A plume model, the hybrid single-particle Lagrangian integrated trajectory (HYSPLIT—Draxler and Hess, 1998) model was run for the ACURATE period using the same meteorological data as the 3D global model calculation.

In HYSPLIT, the computation is composed of three components: particle transport by the mean wind, a turbulent transport component, and the computation of air concentration. Pollutant particles are released at the source location and passively follow the wind. The mean particle trajectory is the integration of the particle position vector in space and time. The turbulent component of the motion defines the dispersion of the pollutant cloud and it is computed by adding a random component to the mean advection velocity in each of the 3D wind component directions. The vertical turbulence is computed from the wind and temperature profiles and the horizontal turbulence is computed from the velocity deformation. Air concentrations are computed by summing each particle's mass as it passes over the concentration grid. The concentration grid is treated as a matrix of cells, each with a volume defined by its dimensions. A detailed description of the model can be found in Draxler and Hess (1997).

The results of the plume calculation at MUH can be seen in Fig. 6, which shows the concentration time series for the HYSPLIT calculation as well as the measured plume using the variable background subtraction method. The first half of ACURATE (1982) shows much larger measured and calculated plumes than the last half (1983). Although the magnitudes of the measured and calculated plumes are comparable, the number of calculated plumes exceeds the number of measured plumes. It is uncertain if these results are due to the use of coarse resolution meteorological data to resolve plume transport directions or if there could be inaccuracies in the hourly emission inventory used for the plume calculation.

Another aspect to these results is that the HYSPLIT calculation shows multiple small plume signals less than 1 pCi m^{-3} that are also evident in the variable background plume. This supports the earlier contention that there is a lot of plume signal buried in what was previously considered to be random background fluctuations. Although the constant median background plume calculation would yield a similar number of small plume events as the variable background subtraction method, the correlation coefficients between the HYSPLIT plume calculation and any of the background

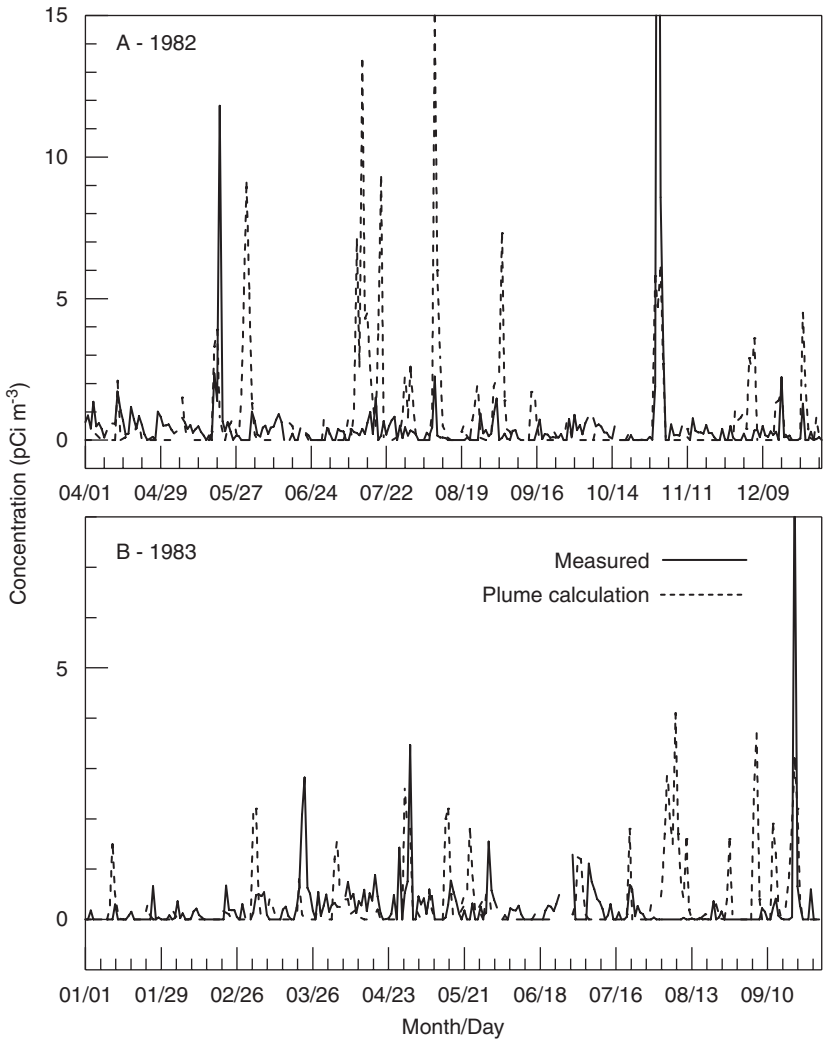

Fig. 6. The SRP plume concentration time series for 1982 (top panel A) and 1983 (bottom panel B) at MUH using the variable background subtraction method (solid line) and the HYSPLIT calculated plume (dotted line). Note the difference in the ordinate scale between 1982 and 1983.

subtraction method plumes are too small and all insignificantly different from each other to determine if they are comparable. The strength in the 3D modeling approach in estimating plumes is that it does not rely upon a large time series of sampling data with a pre-conceived statistical distribution to determine the background concentration at a specific location.

Another way to examine these results is to look at the cumulative frequency distribution of the model and measured plume values using the different background subtraction methods. These results are shown in Table 7. HYSPLIT shows over-prediction

Table 7
The cumulative frequency distribution of concentration at MUH calculated by HYSPLIT and measured using the original constant background subtraction method, the median background subtraction, and the new variable background subtraction

Percentile	Calculated ($pCi\,m^{-3}$)	Constant ($pCi\,m^{-3}$)	Median ($pCi\,m^{-3}$)	Variable ($pCi\,m^{-3}$)
99^{th}	7.10	2.70	3.20	3.47
95^{th}	2.60	0.30	0.80	1.00
90^{th}	1.70	0.00	0.50	0.72
75^{th}	0.30	0.00	0.30	0.41
50^{th}	0.00	0.00	0.10	0.14

of the highest concentrations but indicates a much better approximation of the mid-range percentiles of the distribution than the original constant background subtraction method. The variable background approach also shows somewhat higher concentrations, more similar to the HYSPLIT calculation than the constant median background approach.

6. Summary

A global 3D transport–dispersion model was used to simulate ^{85}Kr background concentrations at five sampling locations that were used to monitor the ^{85}Kr plume 300–1000 km from the SRP during 1982–1983. In the original analyses of the measurements, a constant value representing an upper-limit to the background concentration and different for each station, was subtracted from the measurements to obtain the part of the measurement representing the SRP plume. Due to the long half-life of ^{85}Kr most of the measurement represents the accumulated emissions since the beginning of nuclear fuel reprocessing, or about 18 pCi m^{-3} during this period. Additional variations on the order of 1 pCi m^{-3} can be attributed to very long-range contributions from recent emissions from the major northern hemisphere source points. Finally, the SRP plume signal of a few pCi m^{-3} at the more distant stations is superimposed on top of these variations. Using emission estimates from each of the known ^{85}Kr sources, a 3D global model was used to estimate the daily air concentration variations at the sampling locations from all the sources except the SRP. One limitation to this approach is that although emissions may be relatively well known on an annual basis, unknown shorter term temporal variations in emission rates also contribute to the day-to-day concentration fluctuations observed in the measurements. Nevertheless, the correlation of the 3D model prediction with the measurements ranged from 0.36 to 0.46. The 3D model prediction was then subtracted from the measured air concentrations, resulting in a concentration time series representing the SRP plume. This new method indicated about twice as much of the measured signal could be attributed to the SRP than when using the original constant background subtraction for the most distant samplers.

References

Bey, I., Jacob, D.J., Yantosca, R.M., Logan, J.A., Field, B., Fiore, A.M., Li, Q., Liu, H., Mickley, L.J., Schultz, M., 2001. Global modeling of tropospheric chemistry with assimilated meteorology: model description and evaluation. Journal of Geophysical Research 106, 23073–23095.

Draxler, R.R., Hess, G.D., 1997. Description of the HYSPLIT_4 modeling system. NOAA Technical Memo, ERL ARL-224, 24pp. (NTIS PB98-116593).

Draxler, R.R., Hess, G.D., 1998. An overview of the HYSPLIT_4 modelling system for trajectories, dispersion, and deposition. Australian Meteorological Magazine 47, 295–308.

Draxler, R.R., Dietz, R., Lagomarsino, R.J., Start, G., 1991. Across North America tracer experiment (ANATEX): sampling and analysis. Atmospheric Environment 25A, 2815–2836.

Ferber, G.J., Telegadas, K., Heffter, J.L., Smith, M.E., 1977. Air concentrations of Krypton-85 in the Midwestern United States during January–May 1974. Atmospheric Environment 11, 379–385.

Heffter, J.L., Schubert, J.F., Meade, G.A., 1984. Atlantic Coast Unique Regional Atmospheric Tracer Experiment. NOAA Technical Memo, ERL ARL-130, 15pp. plus appendices.

Horowitz, L.W., Walters, S., Mauzerall, D.L., Emmons, L.K., Rasch, P.J., Granier, C., Tie, Lamarque, J.F., Schultz, M.G., Brasseur, G.P., 2004. A global simulation of tropospheric ozone and related tracers: description and evaluation of MOZART, version 2. Journal of Geophysical Research 108, 4784–4812.

Jacob, D.J., Prather, M.J., Wofsy, S.C., McElroy, M.B., 1987. Atmospheric distribution of ^{85}Kr simulated with a general circulation model. Journal of Geophysical Research 92, 6614–6626.

Kalnay, E., Kanamitsu, M., Kistler, R., Collins, W., Deaven, D., Gandin, L., Iredell, M., Saha, S., White, G., Woollen, J., Zhu, Y., Chelliah, M., Ebisuzaki, W., Higgins, W., Janowiak, J., Mo, K.C., Ropelewski, C., Wang, J., Leetmaa, A., Reynolds, R., Jenne, R., Joseph, D., 1996. The NCEP/NCAR 40-year reanalysis project. Bulletin of the American Meteorological Society 77, 437–471.

Levin, I., Hesshaimer, V., 1996. Refining of atmospheric transport model entries by the globally observed passive tracer distributions of ^{85}krypton and sulfur hexafluoride (SF6). Journal of Geophysical Research 101, 16745–16755.

Mosca, S., Graziani, G., Klug, W., Bellasio, R., Bianconi, R., 1998. A statistical methodology for the evaluation of long-range dispersion models: an application to the ETEX exercise. Atmospheric Environment 32, 4307–4324.

Pendergast, M.M., Boni, A.L., Ferber, G.J., Telegadas, K., 1979. Measured weekly ^{85}Kr concentrations within 150 km of the Savannah river plant (March 1975–August 1976), SRI, DP-1486, NTIS Springfield, VA, 56pp.

Phillips, N.A., 1986. Turbulent mixing near the ground for the Nested Grid Model. Office Note 318, National Meteorological Center, National Weather Service, Silver Spring, MD, 19pp.

Prather, M., McElroy, M., Wofsy, S., Russell, G., Rind, D., 1987. Chemistry of the global troposphere: fluorocarbons as tracers of air motion. Journal of Geophysical Research 92, 6579–6613.

Telegadas, K., Ferber, G.J., Draxler, R.R., Pendergast, M.M., Boni, A.L., Hughes, J., Gray, J., 1980. Measured weekly and twice-daily Krypton-85 surface air concentrations within 150 km of the Savannah river plant (March 1975–September 1977) Final Report. NOAA Technical Memo. ERL ARL-80, 97pp.

Weiss, W., Sittkus, A., Stockburger, H., Sartorius, H., 1983. Large-scale atmospheric mixing derived from meridional profiles of Krypton 85. Journal of Geophysical Research 88, 8574–8578.

Winger, K., Feichter, J., Kalinowski, M.B., Sartorius, H., Schlosser, C., 2005. A new compilation of the atmospheric ^{85}krypton inventories from 1945 to 2000 and its evaluation in a global transport model. Journal of Environmental Radioactivity 80, 183–215.

World Meteorological Organization (WMO), 1995. Report of an expert consultation on ^{85}Kr and ^{222}Rn: measurements, effects and applications. Environmental Pollution Monitoring and Research Programme Report Series No. 109, Geneva, Switzerland, WMO/TD No. 733, 35pp.

Zimmermann, P.H., Feichter, J., Rath, H.L., Crutzen, P.J., Weiss, W., 1989. A global three-dimensional source–receptor model investigation using ^{85}Kr. Atmospheric Environment 23, 25–35.